Національна академія наук України

ІНСТИТУТ ФІЗИКИ КОНДЕНСОВАНИХ СИСТЕМ

ICMP–20–09E

I. Kravtsiv, T. Patsahan, M. Holovko, D. Di Caprio*

SOFT PARTICLE FLUID WITH COMPETING INTERACTIONS AT A HARD WALL: FIELD THEORY APPROACH

*Institut de Recherche de Chimie Paris, CNRS— Chimie ParisTech, 11 rue Pierre et Marie Curie, 75005 Paris, France

ЛЬВІВ

УДК: 536; 536.77; 536.71.

PACS: 05.20.Jj, 05.70.Np, 61.20.-p, 68.03.-g

Плин м'яких частинок із конкуруючими взаємодіями поблизу твердої поверхні: теоретико-польовий підхід

І. Кравців, Т. Пацаган, М. Головко, Д. ді Капріо

Анотація. Розглянуто модель конкуруючої міжчастинкової взаємодії у формі потрійного потенціалу Юкави. Комп'ютерне моделювання системи показало, що запропонована модель здатна описувати спонтанне виникнення в системі мезоструктурованих фаз різної морфології. Зазначені явища самоорганізації стають більш вираженими за присутності обмежуючих поверхонь. Для вивчення структури та термодинаміки мезоскопічно однорідного плину в об'ємній області та поблизу твердої поверхні, застосовано теоретико-польовий підхід. Отримано явні аналітичні вирази для парної кореляційної функції та профілю густини. Означено характерний твердий радіус формально м'яких частинок і розраховано структурний фактор, на основі якого побудовано λ-лінії та досліджено фазову поведінку.

Soft particle fluid with competing interactions at a hard wall: field theory approach

I. Kravtsiv, T. Patsahan, M. Holovko, D. Di Caprio

Abstract. A model of competing pair interaction in the form of a three-Yukawa (3Y) potential is considered. The results of computer simulations show that the model proposed can describe spontaneous appearance in a homogeneous fluid of a large variety of mesostructured phases. Furthermore, these self-assembly effects appear to be favored by the presence of confining walls. To study the structure and thermodynamics of a mesoscopically homogeneous 3Y fluid in the bulk and close to a hard wall, a field theory approach is subsequently applied. Explicit analytical expressions for the pair correlation function and the density profile are derived. The structure factor is calculated by introducing an effective hard core radius characteristic of the system, based on which the λ-lines are constructed and phase behavior discussed.

Подається в Journal of Molecular Liquids
Submitted to Journal of Molecular Liquids

Препринти Інституту фізики конденсованих систем НАН України розповсюджуються серед наукових та інформаційних установ. Вони також доступні по електронній комп'ютерній мережі на WWW-сервері інституту за адресою http://www.icmp.lviv.ua/

The preprints of the Institute for Condensed Matter Physics of the National Academy of Sciences of Ukraine are distributed to scientific and informational institutions. They also are available by computer network from Institute's WWW server (http://www.icmp.lviv.ua/)

Іван Ярославович Кравців
Тарас Миколайович Пацаган
Мирослав Федорович Головко
Дунг ді Капріо

Плин м'яких частинок із конкуруючими взаємодіями поблизу твердої поверхні: теоретико-польовий підхід

Роботу отримано 14 грудня 2020 р.

Затверджено до друку Вченою радою ІФКС НАН України

Рекомендовано до друку відділом теорії м'якої речовини

Виготовлено при ІФКС НАН України

1. Introduction

Models of fluids with competing interactions, which are characterized by short-range attraction and long-range repulsion (the so-called SALR potential), have been the focus of extensive research due to their ability to describe spontaneous emergence in a homogeneous fluid of mesostructured phases of different morphologies [1]. Such potentials are of coarse-grained nature and are often used to model effective solvent-mediated interaction between complex molecules.

For systems with competing interactions in the bulk a large body of research has been reported, yet far fewer results exist for spatially confined systems. Even for the bulk case, most studies have been done in the framework of phenomenological approaches such as Landau-Brazowski theory [2], which make it difficult to link microscopic parameters of the system to respective measurable quantities. Confined systems have typically been investigated in two dimensions [3], although some results for the three dimensional case have also been reported. In [4] a hard core two-Yukawa fluid confined in a slit-like pore was studied. In [5] the structure and adsorption of a system with competing interactions confined by an attractive wall was considered.

We propose to study a fluid interacting with a three-Yukawa potential of the SALR form. Such a model with a soft core takes into account the possibility of partial overlap between two particles. Examples of such systems include, but are not limited to, protein molecules, soft colloids, polymer grafted nanoparticles, star and branched polymers, microgels. Such a potential also has the advantage of being analytical, which makes it possible to perform analytical calculations.

Using computer simulations, we have examined the system under consideration in a wide range of density and temperature values. We show that at low temperatures various well-known mesostructures, such as lamellar and gyroidal phases, hexagonally packed cylindrical phases, cubically ordered and disordered clusters [6–9], are formed. In the case of the system confined between two hard walls, the self-assembly effects become more pronounced may be observed at temperatures that are noticeably higher than in the bulk.

To describe structural properties of a 3Y fluid at high temperatures, a classical field theory [10, 11] is employed. As a first step, we present theoretical results for the mesoscopically homogeneous phase in contact with a hard wall. Explicit analytical expressions for the pair correlation function and the density profile are derived. The results found are tested against computer simulations data.

2. The model

We study a fluid of soft particles interacting with a Three-Yukawa (3Y) potential given by

$$\nu(r) = \frac{A_1}{r}\exp(-\alpha_1 r) + \frac{A_2}{r}\exp(-\alpha_2 r) + \frac{A_3}{r}\exp(-\alpha_3 r), \qquad (2.1)$$

where r denotes the distance between two particles, A_i are the amplitudes of interaction and α_i are the inverse ranges. We choose the values of these parameters so as to reproduce the SALR (short-range attractive and long-range repulsive) potential. We therefore assume that $A_1 > 0$, $A_2 < 0$, $A_3 > 0$ and $|A_1| > |A_2| > |A_3|$, $\alpha_1 > \alpha_2 > \alpha_3$.

Hence, we consider two sets of parameters which we will refer to as Models M1 ($A_1 = 92.1106$, $\alpha_1 = 1.463485$, $A_2 = -81.91964$, $\alpha_2 = 1.0$, $A_3 = 16.07036$, $\alpha_3 = 0.6$) and M2 ($A_1 = 150.6561$, $\alpha_1 = 1.923254$, $A_2 = -122.613$, $\alpha_2 = 1.26115$, $A_3 = 27.11811$, $\alpha_3 = 0.75669$). The respective shapes of these potentials are shown in Figure 1. We note that the Model M2, shown by the red dashed line, displays stronger long-range repulsion relative to the Model M1.

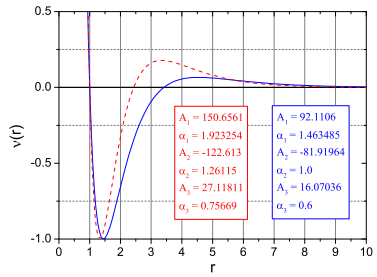

Figure 1. Pair interaction potential (2.1) corresponding to M1 (lower line) and M2 (upper line) sets of parameter values

Due to the softness of the core, the potential (2.1) makes it possible to take into account partial overlap between particles. The model can, therefore, describe effective pair interaction in a variety of soft matter systems such as star-polymer blends, dispersions of polymer-grafted nanoparticles, solutions of proteins, and microgel suspensions. In addition, the potential is convenient for analytical calculations as well as molecular dynamics computer simulations.

3. Computer simulations

A series of Monte-Carlo (MC) and Molecular Dynamics (MD) computer simulations have been performed to investigate whether Models M1 and M2 can describe micro-segregation phenomena and to estimate the ranges of temperatures and densities at which they occur. In addition, we were interested in the confinement effects for such systems. Having the intention to study purely the impact of confinement, we considered the case with no attraction between the walls and the particles.

In Figure 2 we present simulation snapshots for the Model M1 in the bulk. For comparison, Figure 3 shows simulation snapshots for the same system confined between two inert walls. One can see that at $T = 10.0$ the bulk fluid is uniform, while near the walls distinct clusters of particles are formed. As the temperature is raised, at $T = 12.0$ clusters disappear; however, some inhomogeneties at the walls still persist. From these facts we infer that confining walls trigger and favor micro-segregation effects for fluids with competing interactions.

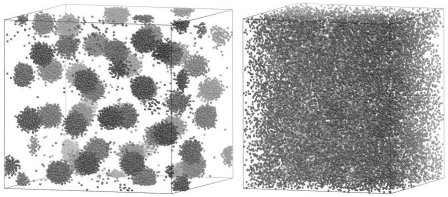

Figure 2. MC snapshots in the bulk (Model M1) at $T = 8.0$, $\rho = 0.25$ (left) and $T = 10.0$, $\rho = 0.25$ (right).

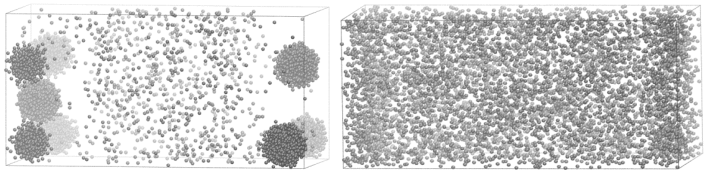

Figure 3. MC snapshots for a fluid confined between two hard walls (Model M1) at $T = 10.0$, $\rho = 0.25$ (left) and $T = 12.0$, $\rho = 0.25$ (right). The walls are located on the left and right edges of the box.

In Figures 4 and 5 some simulation snapshots for the Model M2 in

the bulk are presented. Due to the fact that potential M2 is stronger than M1, the respective systems show richer phenomenological behavior. At high temperatures a uniform fluid is observed. As the temperature is decreased, the model exhibits spontaneous appearance in the system of a wide variety of mesostructures including lamellar and gyroid phases, hexagonal packed cylindrical phases, cubically ordered and disordered clusters formed by particles as well as voids.

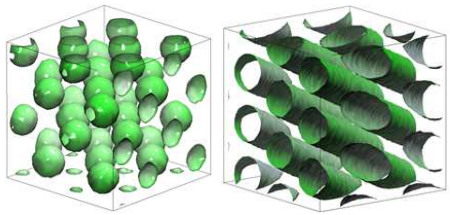

Figure 4. MC snapshots for a bulk fluid (Model M2). BCC lattice of spherical clusters (left) and hexagonal ordered cylinders (right)

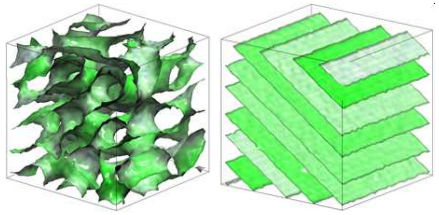

Figure 5. MC snapshots for a bulk fluid (Model M2). Gyroid (left) and lamellar (right) structures.

A phase transition to a modulated inhomogeneous phase can also be seen in the plots of the pair distribution function $g(r)$ for the bulk M2 fluid and the density profile for a fluid at a confining wall (Figures 6 and 7). At higher temperatures, the function $g(r)$ displays a weak peak and rapidly tends to its asymptotic value of unity. However, for lower temperatures $g(r)$ significantly enhances its value over a large length scale indicative of the cluster radius. For all the temperatures, the density profiles are characterized by distinct double maxima close to the wall. At higher temperatures the profile decays to its bulk value, while at lower temperatures the density displays oscillations signaling the presence of

large scale ordering in the system. These effects are more pronounced in the case of higher density $\rho = 0.75$ (Fig. 7), which at $T = 2.0$ corresponds to a lamellar structure (Fig. 5 on the right) and less prominent for a fluid with $\rho = 0.25$ (Fig. 6) corresponding to a spherical cluster phase at $T = 2.0$ (Fig. 4 on the left).

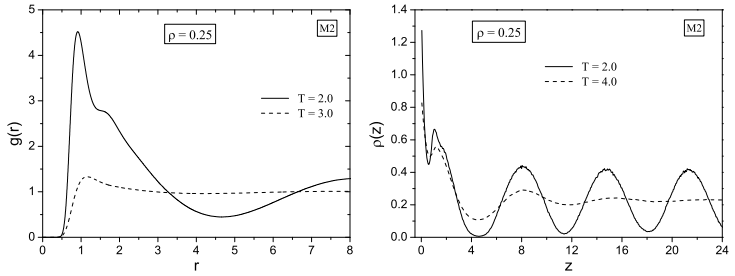

Figure 6. The pair distribution function (left) for a bulk fluid and the density profile for a fluid confined by a hard wall (right) for M2 parameters at $\rho = 0.25$. The temperature $T = 2.0$ corresponds to a spherical cluster phase. The results have been obtained from computer simulations.

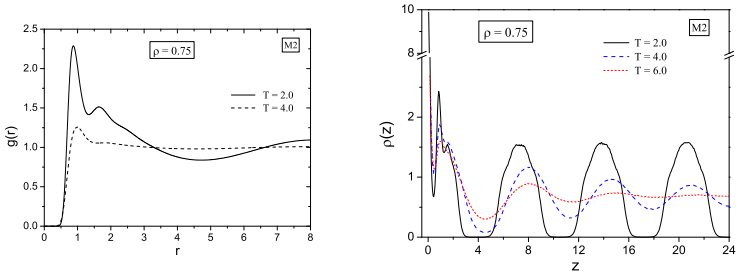

Figure 7. Same as in Figure 6 for $\rho = 0.75$. The temperature $T = 2.0$ corresponds to a lamellar structure.

The aim of the present paper is to show that the soft core SALR potential (2.1) can describe spontaneous transition of a homogeneous fluid to mesoscopically inhomogeneous phases and to explore structural properties of such a fluid in the bulk and in the vicinity of a confining wall. In a series of papers on fluids with specific interactions [10–18], we

show that it is possible to describe these systems using a field theoretical approach. To reproduce density profiles found from computer simulations and as a first step toward field theoretical description of fluids with competing interactions, in the present paper we apply this method to a fluid with the pair potential (2.1) in the mesoscopically homogeneous region of the phase space.

4. Field theoretical approach

In the framework of the field theory (FT) formalism, the Hamiltonian of a classical system is a functional of the density field $\rho(\mathbf{r})$ and is expressed as the sum of an entropic and an interaction terms

$$\beta H[\rho(\mathbf{r})] = \beta H^{entr}[\rho(\mathbf{r})] + \beta H^{int}[\rho(\mathbf{r})], \tag{4.1}$$

which respectively have the forms

$$\beta H^{entr}[\rho(\mathbf{r})] = \int \rho(\mathbf{r}) \left(\ln\left[\rho(\mathbf{r})\Lambda^3\right] - 1\right) d\mathbf{r} \tag{4.2}$$

$$\beta H^{int}[\rho(\mathbf{r})] = \frac{\beta}{2}\int \nu(r)\Big[\rho(\mathbf{r}_1)\rho(\mathbf{r}_2) - \rho(\mathbf{r}_1)\delta(\mathbf{r}_1-\mathbf{r}_2)\Big] d\mathbf{r}_1 d\mathbf{r}_2, \tag{4.3}$$

where k_B is the Boltzmann constant, $\beta = 1/k_BT$ is the inverse temperature, $\nu(r)$ is the potential of interaction between two particles at points 1 and 2, and $\delta(\mathbf{r})$ is the Dirac function.

In the present work the calculations are carried out in the framework of the canonical ensemble approach. For this reason we are interested in the partition function Z_N of the system, which is expressed as

$$Z_N\left[\rho(\mathbf{r})\right] = \int D\rho(\mathbf{r}) \exp\{-\beta H[\rho(\mathbf{r})]\}. \tag{4.4}$$

The number of particles is fixed by the condition $\int \rho(\mathbf{r})d\mathbf{r} = N$ or $\frac{1}{V}\int \rho(\mathbf{r})d\mathbf{r} = \rho$, where V is the volume and $\rho = N/V$ is the average density. To ensure this condition, we define a Lagrange multiplier λ such that

$$\frac{\delta\beta H[\rho(\mathbf{r})]}{\delta\rho(\mathbf{r})} = \lambda. \tag{4.5}$$

The logarithm of the partition function gives the Helmholtz free energy

$$\beta F = -\ln Z_N. \tag{4.6}$$

The lowest order approximation for the partition function is the saddle point approximation for the functional integral (4.4), which corresponds to the mean field (MF) approximation from the physical standpoint. The MF approximation thus corresponds to the condition

$$\left.\frac{\delta\beta H}{\delta\rho}\right|_{\rho^{MF}(\mathbf{r})} = \lambda. \tag{4.7}$$

In order to take into account fluctuations one should expand the Hamiltonian around the field $\rho^{MF}(\mathbf{r})$, i.e. write $\rho(\mathbf{r}) = \rho^{MF}(\mathbf{r}) + \delta\rho(\mathbf{r})$. In general, this leads to the following expression for the Hamiltonian

$$\beta H[\rho] = \beta H\left[\rho^{MF}\right] + \int \delta\rho(\mathbf{r_1}) \left.\frac{\delta\beta H}{\delta(\delta\rho(\mathbf{r_1}))}\right|_{\rho^{MF}} d\mathbf{r_1} + \tag{4.8}$$

$$\frac{1}{2}\int \delta\rho(\mathbf{r_1})\delta\rho(\mathbf{r_2}) \left.\frac{\delta^2\beta H}{\delta(\delta\rho(\mathbf{r_1}))\delta(\delta\rho(\mathbf{r_2})}\right)\Big|_{\rho^{MF}} d\mathbf{r_1}d\mathbf{r_2} +$$

$$\sum_{n\geq 3}(-1)^n\frac{(n-1)!}{n!}\int \delta\rho(\mathbf{r_1})\ldots\delta\rho(\mathbf{r_n}) \left.\frac{\delta^n\beta H}{\delta(\delta\rho(\mathbf{r_1}))\ldots\delta(\delta\rho(\mathbf{r_n})}\right)\Big|_{\rho^{MF}} d\mathbf{r_1}\ldots d\mathbf{r_n}.$$

The first term corresponds to the functional (4.1) for the mean field density

$$\beta H[\rho^{MF}] = \int \rho^{MF}(\mathbf{r_1}) \left(\ln\left[\rho^{MF}(\mathbf{r_1})\Lambda^3\right] - 1\right) d\mathbf{r_1} \tag{4.9}$$

$$+ \frac{\beta}{2}\int \nu(\mathbf{r}_1,\mathbf{r}_2)\Big[\rho^{MF}(\mathbf{r_1})\rho^{MF}(\mathbf{r_2}) - \rho^{MF}(\mathbf{r}_1)\delta(\mathbf{r}_1-\mathbf{r}_2)\Big] d\mathbf{r_1}d\mathbf{r_2}.$$

The linear term disappears as in the canonical ensemble the fluctuations preserve the number of particles and $\int \delta\rho(\mathbf{r})d\mathbf{r} = 0$. The terms of higher orders come from the expansion of the logarithm in the expression (4.2).

5. Three-Yukawa fluid in the bulk

In this section we apply field theory to study analytically the properties of a 3Y fluid in the bulk region. One point of interest is to investigate the conditions for the appearance of inhomogeneous phases, which is signaled by the divergence of the structure factor $S(k)$. The curve separating the respective homogeneous and inhomogeneous phases (known as the λ-line) is therefore determined by the locus of points on the phase diagram, at which $S(k)$ diverges. This knowledge is also important for numerical calculations of the density profiles which we intend to perform within the homogeneous part of the phase diagram. In addition, it is instrumental to know whether the model under consideration exhibits liquid-vapor phase separation.

5.1. The pair distribution function

The structure of a fluid can be described by the pair distribution function $g(r) = 1+h(r)$, where $h(r)$ is the pair correlation function. This quantity can be found from the following expression [19]

$$h(\mathbf{r}_1, \mathbf{r}_2)\langle\rho(\mathbf{r}_1)\rangle\langle\rho(\mathbf{r}_2)\rangle = \langle\delta\rho(\mathbf{r}_1)\delta\rho(\mathbf{r}_2)\rangle - \delta\left(\mathbf{r}_1 - \mathbf{r}_2\right)\langle\rho(\mathbf{r}_1)\rangle. \quad (5.1)$$

We expand the Hamiltonian with respect to the mean field density $\rho^{MF}(\mathbf{r})$. Truncation of expansion (4.8) at the second term corresponds to the description of the system in the Gaussian approximation.

The quadratic term in Eq. (4.8) is

$$\beta H_2[\rho] = \frac{1}{2}\int \delta\rho(\mathbf{r_1})\delta\rho(\mathbf{r_2})\left[\frac{\delta(\mathbf{r}_1 - \mathbf{r}_2)}{\rho^{MF}(\mathbf{r_1})} + \beta\nu(r)\right] d\mathbf{r_1} d\mathbf{r_2}, \quad (5.2)$$

where the first term comes from the expansion of the logarithm in the entropic part of the Hamiltonian.

In order to calculate the averages using the Gaussian integrals, it is necessary to have the quadratic term of the Hamiltnian in a diagonal form. For bulk properties we can expand the density on the Fourier components

$$\delta\rho(\mathbf{r}) = \sum_{\mathbf{k}>0} \delta\rho_{\mathbf{k}}\, e^{\mathbf{i}\mathbf{k}\mathbf{r}}. \quad (5.3)$$

In this basis the quadratic Hamiltonian equals

$$\beta H_2[\rho] = \frac{V}{2\rho}\sum_{\mathbf{k}>0} \delta\rho_{\mathbf{k}}\delta\rho_{-\mathbf{k}}\left[1 + \nu(k)\right], \quad (5.4)$$

where

$$\nu(k) = \sum_{i=1}^{3} \frac{4\pi\beta A_i}{k^2 + \alpha_i^2} \quad (5.5)$$

is the Fourier transform of the interaction potential (2.1) multiplied by the inverse temperature.

Calculating the averages in (5.1) with the weight given by the quadratic Hamiltonian (5.4), we arrive at the following relation

$$\langle\delta\rho(\mathbf{k})\delta\rho(-\mathbf{k})\rangle = \frac{\int D\left(\delta\rho(\mathbf{k})\right)\, e^{-\beta H_2\left[\rho(\mathbf{k})\right]}\delta\rho(\mathbf{k})\delta\rho(-\mathbf{k})}{\int D\left(\delta\rho(\mathbf{k})\right)\, e^{-\beta H_2\left[\rho(\mathbf{k})\right]}} \quad (5.6)$$

The Fourier transform of the pair correlation function is then

$$h(k) = -\frac{\beta\nu(k)}{1 + \rho\beta\nu(k)} = -\frac{1}{\rho}\frac{P(k)}{D(k)}. \quad (5.7)$$

The numerator and denominator on the RHS of equation (5.7) equal, respectively,

$$P(k) = \varkappa_1^2(k^2+\alpha_2^2)(k^2+\alpha_3^2) + \varkappa_2^2(k^2+\alpha_1^2)(k^2+\alpha_3^2) + \varkappa_3^2(k^2+\alpha_1^2)(k^2+\alpha_2^2), \quad (5.8)$$

$$\begin{aligned} D(k) = {} & k^6 + k^4(\tilde{\varkappa}_1^2 + \tilde{\varkappa}_2^2 + \tilde{\varkappa}_3^2) \\ & + k^2\left[\tilde{\varkappa}_1^2\tilde{\varkappa}_2^2 + \tilde{\varkappa}_1^2\tilde{\varkappa}_3^2 + \tilde{\varkappa}_2^2\tilde{\varkappa}_3^2 - \varkappa_1^2\varkappa_2^2 - \varkappa_1^2\varkappa_3^2 - \varkappa_2^2\varkappa_3^2\right] \\ & + \alpha_1^2\alpha_2^2\alpha_3^2 + \varkappa_1^2\alpha_2^2\alpha_3^2 + \varkappa_2^2\alpha_1^2\alpha_3^2 + \varkappa_3^2\alpha_1^2\alpha_2^2, \end{aligned} \quad (5.9)$$

where $\tilde{\varkappa}_i^2 = \varkappa_i^2 + \alpha_i^2$.

Taking the inverse Fourier transform of expression (5.7), we can find $h(r)$

$$h(r) = \frac{1}{(2\pi)^3}\int_{-\infty}^{\infty} \mathbf{d}\mathbf{k} h(k)\exp\left(-i\mathbf{k}\mathbf{r}\right). \quad (5.10)$$

In order to perform analytical integration in Eq. (5.10), one needs to factorize the denominator $D(k)$. To this end, we need to solve the bicubic equation $D(k) = 0$.

5.2. Solution of the bicubic equation

Equation $D(k) = 0$ can be presented in a cubic form

$$K^3 + bK^2 + cK + d = 0, \quad (5.11)$$

where

$$K = k^2; \quad (5.12)$$

$$b = (\tilde{\varkappa}_1^2 + \tilde{\varkappa}_2^2 + \tilde{\varkappa}_3^2); \quad (5.13)$$

$$c = \left[\tilde{\varkappa}_1^2\tilde{\varkappa}_2^2 + \tilde{\varkappa}_1^2\tilde{\varkappa}_3^2 + \tilde{\varkappa}_2^2\tilde{\varkappa}_3^2 - \varkappa_1^2\varkappa_2^2 - \varkappa_1^2\varkappa_3^2 - \varkappa_2^2\varkappa_3^2\right] \quad (5.14)$$

$$d = \tilde{\varkappa}_1^2\left[\tilde{\varkappa}_2^2\tilde{\varkappa}_3^2 - \varkappa_2^2\varkappa_3^2\right] - \varkappa_1^2\varkappa_2^2\tilde{\varkappa}_3^2 - \varkappa_1^2\varkappa_3^2\tilde{\varkappa}_2^2 + 2\varkappa_1^2\varkappa_2^2\varkappa_3^2. \quad (5.15)$$

The numbers of real and complex roots are determined by the discriminant of the cubic equation,

$$\Delta = 18bcd - 4b^3d + b^2c^2 - 4c^3 - 27d^2. \quad (5.16)$$

If $\Delta > 0$, then the equation has three distinct real roots. If $\Delta = 0$, then the equation has a multiple root and all of its roots are real. If $\Delta < 0$, then the equation has one real root and two non-real complex conjugate roots.

The general solution of the cubic equation involves first calculating:

$$\Delta_0 = b^2 - 3c \tag{5.17}$$

$$\Delta_1 = 2b^3 - 9bc + 27d, \tag{5.18}$$

$$C = \sqrt[3]{\frac{\Delta_1 \pm \sqrt{{\Delta_1}^2 - 4{\Delta_0}^3}}{2}} = \sqrt[3]{\frac{\Delta_1 \pm \sqrt{-27\Delta}}{2}} \tag{5.19}$$

There are three possible cube roots implied by the expression, of which at least two are non-real complex numbers; any of these may be chosen when defining C. In addition, either sign in front of the square root may be chosen unless Δ_0 in which case the sign must be chosen so that the two terms inside the cube root do not cancel.

We consider the case when the cubic equation (6.25) produces one real solution k_0^2 and a pair of complex conjugate solutions k_1^2 and k_2^2. For C we choose a plus in front of the square root. For the region of parameter values considered, the resulting expression under the cube root is positive, therefore C can take on three values: a real positive number or one of the two complex conjugate numbers. We choose the real positive root to define C:

$$C = \sqrt[3]{\frac{\Delta_1 + \sqrt{-27\Delta}}{2}} \tag{5.20}$$

The solution of the cubic equation can be expressed compactly including all 3 roots as follows:

$$k_j^2 = -\frac{1}{3}\left(b + \xi^j C + \frac{\Delta_0}{\xi^j C}\right), \qquad j \in \{0, 1, 2\}, \tag{5.21}$$

where $\xi = -1/2 + 1/2\sqrt{3}i$ (which is a cube root of unity).

The real solution of the cubic equation appears at $j = 0$:

$$k_0^2 = -\frac{1}{3}\left(b + C + \frac{\Delta_0}{C}\right) \tag{5.22}$$

The complex conjugate solutions appear at $j = 1$ and $j = 2$.

For the parameters under consideration, the solution k_0^2 is a negative quantity. Due to this, we introduce a more convenient set of notations

$$\lambda_j^2 = -k_j^2, \qquad j \in \{0, 1, 2\}. \tag{5.23}$$

The quantities λ_j^2 are essentially the solutions of the cubic equation (6.25) but of the opposite sign. Therefore, they can be written as

$$\lambda_0^2 = \frac{1}{3}\left(b + C + \frac{\Delta_0}{C}\right) \tag{5.24}$$

$$\lambda_1^2 = M_1 + M_2 i, \tag{5.25}$$

$$\lambda_2^2 = M_1 - M_2 i, \tag{5.26}$$

where

$$M_1 = \frac{1}{3}\left(b - \frac{C}{2} - \frac{\Delta_0}{2C}\right) \tag{5.27}$$

$$M_2 = \frac{1}{3}\frac{\sqrt{3}}{2}\left[C - \frac{\Delta_0}{C}\right]. \tag{5.28}$$

Since the quantities λ_1^2 and λ_2^2 are complex conjugate, so are their roots. We can, therefore, write

$$\lambda_1 = \lambda + i\mu, \tag{5.29}$$

$$\lambda_2 = \lambda - i\mu, \tag{5.30}$$

where

$$\lambda = \frac{1}{\sqrt{2}}\left[\sqrt{M_1^2 + M_2^2} + M_1\right]^{1/2} \tag{5.31}$$

$$\mu = \frac{\mathrm{signum}(M_2)}{\sqrt{2}}\left[\sqrt{M_1^2 + M_2^2} - M_1\right]^{1/2}. \tag{5.32}$$

The function $D(k)$ can now be written in a factorized form

$$\begin{aligned} D(k) &= (k^2 + \lambda_0^2)(k^2 + \lambda_1^2)(k^2 + \lambda_2^2) \\ &= (k + i\lambda_0)(k - i\lambda_0)(k + i\lambda_1)(k - i\lambda_1)(k + i\lambda_2)(k - i\lambda_2). \end{aligned} \tag{5.33}$$

The real solutions for the bicubic equation are readily found from Eq. (5.22) and equal $\pm\lambda_0$, where

$$\lambda_0 = \sqrt{\frac{1}{3}\left(b + C + \frac{\Delta_0}{C}\right)}. \tag{5.34}$$

From Eq. (5.10), the expression for the pair correlation function is

$$h(r) = -\frac{1}{2\pi\rho}\left(H_0\frac{\exp(-\lambda_0 r)}{r} + [H_1\cos(\mu r) + H_2\sin(\mu r)]\frac{\exp(-\lambda r)}{r}\right), \tag{5.35}$$

$$H_0 = \frac{1}{2\left[\lambda_0^4 - 2\lambda_0^2(\lambda^2-\mu^2) + (\lambda^2+\mu^2)^2\right]}\sum_{i=1}^{3}\varkappa_i^2(\alpha_j^2-\lambda_0^2)(\alpha_k^2-\lambda_0^2), \tag{5.36}$$

$$H_1 = \frac{1}{8\mu^2\lambda^2 + 2\bar{\lambda}_0^{2^2}}\sum_{i=1}^{3}\varkappa_i^2\left[-\bar{\alpha_j^2}\bar{\alpha_k^2} + \bar{\lambda}_0^2(\bar{\alpha_j^2}+\bar{\alpha_k^2}) + 4\mu^2\lambda^2\right], \tag{5.37}$$

$$H_2 = \frac{1}{16\mu^3\lambda^3 + 4\mu\lambda\bar{\lambda}_0^{2^2}}\sum_{i=1}^{3}\varkappa_i^2\left[4\mu^2\lambda^2(\bar{\alpha_j^2}+\bar{\alpha_k^2}) + \bar{\lambda}_0^2(\bar{\alpha_j^2}\bar{\alpha_k^2} - 4\mu^2\lambda^2)\right], \tag{5.38}$$

where $j,k \in \{1,2,3\}$ with $i \neq j \neq k$, and we use the bar to denote shifted quantities $\bar{(...)} = (... - \lambda^2 + \mu^2)$.

Equation (5.35) tells us that the quantities λ_0, λ and μ have the meaning of parameters that characterize the screening of interaction with λ_0 and λ responsible for the decaying and μ responsible for the oscillatory parts of the interaction. We note that for the values of the pair potential considered in this paper, the quantities λ_0, λ and μ are real numbers. In addition, λ_0 and λ are positive.

In the Gaussian approximation, the radial distribution function (RDF) $g(r)$ can be written as

$$g(r) = 1 + h(r). \tag{5.39}$$

From Eq. (5.35) one can see that the function $g(r)$ diverges when $r \to 0$. As we discussed in our previous papers [10, 11], this behavior can be corrected by introducing exponential approximation for the RDF in the form

$$g^{\exp}(r) = \exp\left[h(r)\right]. \tag{5.40}$$

In Figures 8-11 we compare numerical results for the pair distribution function calculated from Equations (5.39) and (5.40) with computer simulations data. The plots are presented for Models M1 and M2 at different densities and temperatures. One can see that the results of the theory are in qualitative agreement with the simulations while quantitative

agreement improves as the temperature rises. We also note the correct behavior of the exponential approximation (5.40) at small distances in contrast to the non-physical behavior of the initial approximation (5.39).

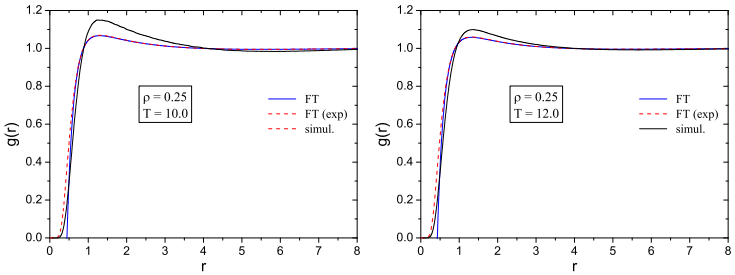

Figure 8. Pair distribution function for Model M1. The blue solid lines are given by Eq. (5.39), the red dashed lines correspond to approximation (5.40), and the black solid curves are calculated from the MC simulations data.

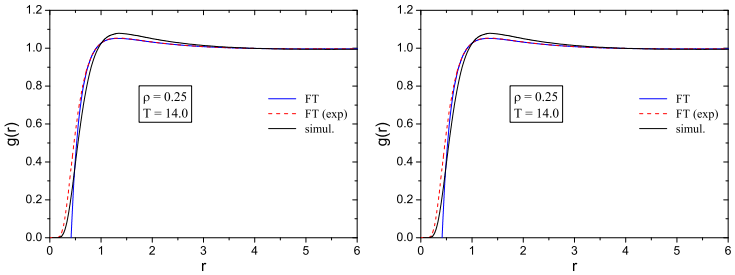

Figure 9. Same as in Figure 8 but at higher temperatures.

5.3. The structure factor and phase coexistence curves

The static structure factor characterizes the microphase structuring displayed by the system. $S(k)$ is given by the expression

$$S(k) = \frac{1}{1-\rho\tilde{c}(k)}, \tag{5.41}$$

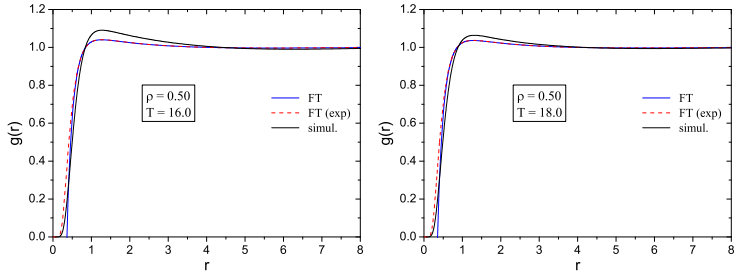

Figure 10. Same as in Figure 8 but for $\rho = 0.50$.

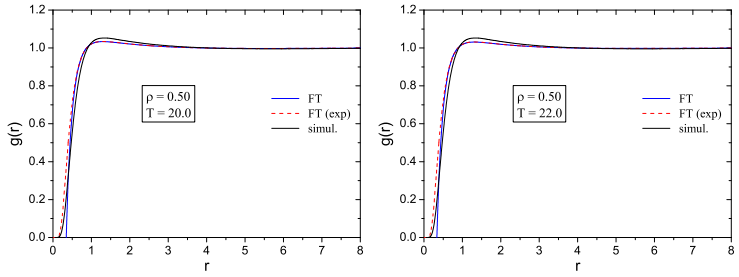

Figure 11. Same as in Figure 10 but at higher temperatures.

where $\tilde{c}(k)$ is the Fourier transform of the direct pair correlation function $c(r)$ of the bulk fluid. In the random phase approximation,

$$\tilde{c}(k) = -\beta\nu(k), \tag{5.42}$$

where $\nu(k)$ is given by Eq. (5.5).

The λ-line is defined as the locus of points in the phase diagram for which the static structure factor $S(k)$ diverges at a particular wave number [24]. We take the λ-line to indicate that the model predicts a phase transition to a modulated inhomogeneous phase. When the fluid is in the homogeneous phase, the denominator $1 - \rho\tilde{c}(k)$ on the RHS of expression (5.41) takes on positive values. As we lower the temperature, the $S(k)$ curve shifts downward and at certain values of the density becomes equal to zero. Therefore, the λ-line can be found from the solution

of the system of equations

$$\rho\tilde{c}(k, \{\rho, T\}) = 1, \tag{5.43}$$

$$\frac{\partial\tilde{c}(k, \{\rho, T\})}{\partial k} = 0. \tag{5.44}$$

For the function $\tilde{c}(k)$ in the form (5.42), the system (5.43)-(5.44) amounts to the following equations

$$(k^2 + \lambda_1^2)(k^2 + \lambda_2^2) = 0, \tag{5.45}$$

$$\sum_{l=1}^{3} \varkappa_l^2 (k^2 + \alpha_m^2)^2 (k^2 + \alpha_n^2)^2 = 0, \tag{5.46}$$

where $m, n \in \{1, 2, 3\}$ and $l \neq m \neq n$.

Due to the fact that in the Equations (5.45)-(5.46) the density and the temperature are present only in the form of the product $\beta\rho$, the solution of this system comes out as a linear equation $\beta\rho = const$. This means that in this case the λ-line is a straight line. In Figure 12 we show the respective result for the model $M1$, while for the model $M2$ the solution lies outside of a reasonable range of density and temperature values. We attribute the non-physical behavior of these results to the weakness of the approximation employed.

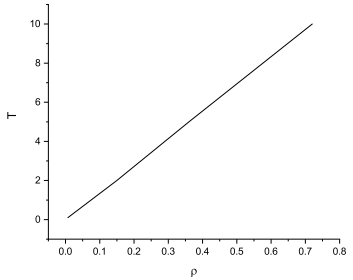

Figure 12. λ-line for model M1 calculated from the direct correlation function given by Eq. (5.42).

Nevertheless, one can show that the model potential (2.1) does, in fact, describe the possibility of the phase transition to a mesoscopically inhomogeneous structure.

Whereas the model of the fluid considered here is formally soft, it can effectively be presented as a system of particles with a hard core [20, 21].

One way to determine the corresponding hard core diameter σ is to use the distance at which the pair potential (2.1) equals the thermal energy k_BT with an arbitrary factor ζ [20], i.e.

$$\nu(r) - \zeta T = 0. \tag{5.47}$$

Another way to determine σ is by employing the Barker-Henderson formula [23]

$$\sigma_{BH} = \int_0^\sigma dr \left(1 - e^{-\beta\nu(r)}\right), \qquad \nu(\sigma) = 0. \tag{5.48}$$

It is reasonable to presume that the value of the effective diameter should stem from the condition that two particles cannot overlap beyond the distance σ, i.e. the distance where the value of the radial distribution function is close to zero. In Figures (13) and (14) we show different estimations of the effective hard core diameter by employing expression (5.47) at $\zeta = 1$ and $\zeta = 4$ as well as the Barker-Henderson recipe (5.48). We analyze the curves of the radial distribution functions given by Equations (5.39) and (5.40) relative to different σ in order to determine the maximum distance, at which the RDF takes on a value close to zero. One can infer that the best approximation corresponds to expression (5.47) with $\zeta \approx 4$. We, therefore, find the value of the effective hard core diameter from the solution of the following equation

$$\nu(r) - 4T = 0. \tag{5.49}$$

Hence, in the framework of the random phase approximation the direct correlation function can be presented as the sum of two parts

$$\tilde{c}(k) = \tilde{c}_{HS}(k) + \tilde{c}_{3Y}(k). \tag{5.50}$$

One part is the effective hard core contribution [22]

$$\tilde{c}_{HS} = -\frac{4\pi}{q^3}\Bigg(a_1\left[\sin q - q\cos q\right] + \frac{6\eta a_2}{q}\left[2q\sin q + (2-q^2)\cos q - 2\right] \tag{5.51}$$

$$+\frac{\eta a_1}{2q^3}\left[4q(q^2-6)\sin q - (24 - 12q^2 + q^4)\cos q + 24\right]\Bigg),$$

where $q = kD$ is a dimensionless wave number, $\eta = \rho\pi\sigma^3/6$ is the packing fraction, and

$$a_1 = \frac{(1+2\eta)^2}{(1-\eta)^4}, \qquad a_2 = -\frac{(1+\eta/2)^2}{(1-\eta)^4}. \tag{5.52}$$

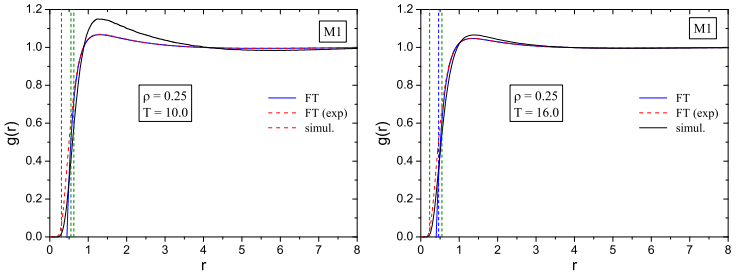

Figure 13. Estimations of the effective hard core diameter for model M1. The green vertical lines correspond to expressions (5.48) and (5.47) at $\zeta = 1$ and $\zeta = 4$, respectively. The blue solid lines depict the radial distribution function given by Eq. (5.39), the red dashed lines correspond to approximation (5.40), and the black solid curves come from the MC simulations data.

The other part of the direct correlation function comes from the long-range potential and can be calculated as

$$\tilde{c}_{3Y}(k) = -\frac{4\pi}{k}\int_\sigma^\infty r\sin(kr)\beta\nu(r)dr \tag{5.53}$$

$$= -4\pi\beta\sum_{l=1}^{3} A_l e^{-\alpha_l\sigma}\left[\{k\cos k\sigma + \alpha_l\sin k\sigma\}\{\alpha_m^2\alpha_n^2 + k^2(\alpha_m^2+\alpha_n^2) + k^3\}\right],$$

where $m, n \in \{1,2,3\}$ and $l \neq m \neq n$.

In Figure (4), left panel, we show the structure factors for models

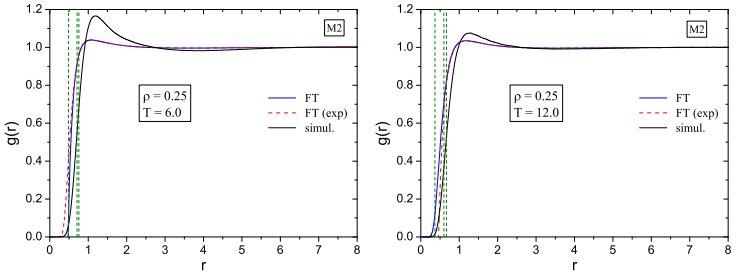

Figure 14. Same as in Figure (13) but for model M2.

M_1 and M_2 with an effective hard core diameter determined from the equation (5.49). One can see distinct pre-peaks signaling the presence of mesoscopic ordering in the system.

On the right panel of Figure (4) we show the respective λ-lines for models $M1$ and $M2$. Both curves have correct shapes, which was not the case when equations (5.45)-(5.46) were considered. We conclude that a correct description of inhomogeneous phases requires one to take into account the excluded volume effects, models with a soft core not being sufficiently accurate. At the same time, the homogeneous phase can be studied without considering an effective hard core model. Having the knowledge of the location of the regions on the phase diagram where there is no micro-segregation and the fluid is uniform, we can safely apply the expressions for the structural properties derived from the field-theoretical approach by substituting the values of the density and the temperature well above the λ-lines.

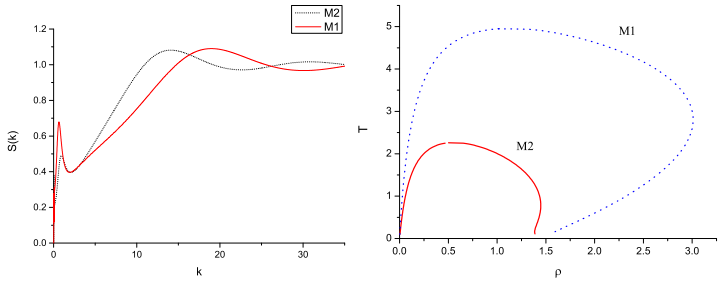

Figure 15. Left: structure factors for models M_1 and M_2 at $\rho = 0.25, T = 10$. Right: λ-lines for models M_1 and M_2.

In this context, another point to consider is related to the vapor-liquid phase separation curves. One way to determine the location of the critical region is to construct the spinodals from the condition

$$\rho\tilde{c}(k = 0, \{\rho, T\}) = 1 \tag{5.54}$$

and see where the critical point lies with respect to the λ-lines. However, the model (5.50) yields no solutions for equation (5.54) for either $M1$ or $M2$. This means that the model fluid studied in this paper does not exhibit vapor-liquid phase transition.

6. Density profiles at a hard wall

In this section we study a three-Yukawa fluid with competing interactions in the vicinity of a hard wall. The potential of interaction between the wall and a particle is taken to be infinite when the distance between them is negative and zero elsewhere.

As expression (4.9) contains the field $\rho^{MF}(\mathbf{r_1})$, one can readily see that in the framework of the FT formalism spatially structured systems can be examined even in the framework of the simplest mean field approximation.

From the mean field condition (4.7) we derive the following equation

$$\ln\frac{\rho(\mathbf{r_1})}{\rho_b} + V_1(\mathbf{r_1}) + V_2(\mathbf{r_1}) + V_3(\mathbf{r_1}) = \lambda \tag{6.1}$$

where potentials $V_i(\mathbf{r_1})$ are defined as

$$V_i(\mathbf{r_1}) = \beta\int \rho(\mathbf{r_2})\frac{A_i}{r}\exp(-\alpha_i r)d\mathbf{r_2}. \tag{6.2}$$

We put

$$\lambda \equiv V_{1b} + V_{2b} + V_{3b}, \tag{6.3}$$

where V_{ib} are the values of potentials $V_i(\mathbf{r}_1)$ in the bulk

$$V_{ib} = \frac{\varkappa_i^2}{\alpha_i^2}, \tag{6.4}$$

$\varkappa_i^2 \equiv 4\pi\rho_b\beta A_i$, and we denote the density of the fluid in the bulk by ρ_b to distinguish it from the distance-dependent density $\rho(z)$ within the interface between the wall and the bulk region.

The gradient of Eq. (6.1) gives

$$\frac{\nabla\rho(\mathbf{r})}{\rho(\mathbf{r})} - \mathbf{E}_1(\mathbf{r}) - \mathbf{E}_2(\mathbf{r}) - \mathbf{E}_3(\mathbf{r}) = 0, \tag{6.5}$$

where we define an equivalent of the electric field by

$$\mathbf{E_i}(\mathbf{r_1}) \equiv -\nabla V_i(\mathbf{r_1}); \tag{6.6}$$

Due to the properties of the Yukawa potential we can write

$$\left(\triangle - \alpha_i^2\right) V_i(\mathbf{r}) = -4\pi\beta A_i\rho(\mathbf{r}). \tag{6.7}$$

Given the translational invariance of the system in the directions parallel to the wall, all the distance-dependent functions in the equations (6.5)-(6.7) are essentially functions of the distance z in the direction perpendicular to the wall. In consequence, from these equations we obtain a set of seven differential equations with seven unknown functions $\rho(z)$, $E_1(z)$, $E_2(z)$, $E_3(z)$, $V_1(z)$, $V_2(z)$, $V_3(z)$:

$$\frac{\partial\rho(z)}{\partial z} = \rho(z)\left[E_1(z)+E_2(z)+E_3(z)\right], \tag{6.8}$$

$$\frac{\partial V_i(z)}{\partial z} = -E_i(z), \tag{6.9}$$

$$\frac{\partial E_i(z)}{\partial z} = -\alpha_i^2 V_i(z) + \frac{\varkappa_i^2}{\rho_b}\rho(z). \tag{6.10}$$

From Eq. (6.1) we have the following equation for the density profile

$$\rho(z) = \rho_b \exp\big(-[V_1(z)-V_{1b}]-[V_2(z)-V_{2b}]-[V_3(z)-V_{3b}]\big). \tag{6.11}$$

Equation (6.11) is an integral equation of the Euler-Lagrange type. Numerical solution of this equation provides the mean field approximation for the density profile of the fluid.

6.1. Analytical expression for the density profile

The density profile can also be estimated in an explicit analytical form. To this end, we approximate the exponent function in Eq. (6.11) as

$$\rho(z) = \rho_b\big(1-[V_1(z)-V_{1b}]-[V_2(z)-V_{2b}]-[V_3(z)-V_{3b}]\big), \tag{6.12}$$

which leads to a linearized system of equations

$$\rho^{'}(z) = \rho_b\left[E_1(z)+E_2(z)+E_3(z)\right], \tag{6.13}$$

$$V_i^{'}(z) = -E_i(z), \tag{6.14}$$

$$E_i^{'}(z) = -\alpha_i^2 V_i(z) + \frac{\varkappa_i^2}{\rho_b}\rho(z). \tag{6.15}$$

In turn, this system can be reduced to a system of three second-order differential equations

$$E_1^{''}(z) = E_1(z)\left(\varkappa_1^2+\alpha_1^2\right) + [E_2(z)+E_3(z)]\varkappa_1^2; \tag{6.16}$$

$$E_2^{''}(z) = [E_1(z)+E_3(z)]\varkappa_2^2 + E_2(z)\left(\alpha_2^2+\varkappa_2^2\right); \tag{6.17}$$

$$E_3^{''}(z) = [E_1(z)+E_2(z)]\varkappa_3^2 + E_3(z)\left(\alpha_3^2+\varkappa_3^2\right), \tag{6.18}$$

or in the matrix form

$$\mathbf{E}^{''} = \mathbf{A}\mathbf{E}, \tag{6.19}$$

where

$$\mathbf{E} = \begin{pmatrix} E_1(z) \\ E_2(z) \\ E_3(z) \end{pmatrix}, \qquad \mathbf{A} = \begin{pmatrix} \left(\varkappa_1^2+\alpha_1^2\right) & \varkappa_1^2 & \varkappa_1^2 \\ \varkappa_2^2 & \left(\alpha_2^2+\varkappa_2^2\right) & \varkappa_2^2 \\ \varkappa_3^2 & \varkappa_3^2 & \left(\alpha_3^2+\varkappa_3^2\right) \end{pmatrix} \tag{6.20}$$

Matrix $\mathbf{A}$ can be presented in the diagonal form as

$$\mathbf{A} = \mathbf{P}\mathbf{D}\mathbf{P}^{-1} \tag{6.21}$$

where

$$\mathbf{D} = \begin{pmatrix} \Lambda_0 & 0 & 0 \\ 0 & \Lambda_1 & 0 \\ 0 & 0 & \Lambda_2 \end{pmatrix}. \tag{6.22}$$

The coefficients Λ_i are the eigenvalues of the matrix $\mathbf{A}$. Denoting the identity matrix as $\mathbf{I}$, we can find these eigenvalues as the roots of the characteristic polynomial of $\mathbf{A}$, i.e. from the equation

$$\det\left(\mathbb{A}-\Lambda\mathbf{I}\right) = 0. \tag{6.23}$$

In our case, this reduces to solving the equation

$$\begin{aligned} &\Lambda^3 - \Lambda^2(\tilde{\varkappa}_1^2+\tilde{\varkappa}_2^2+\tilde{\varkappa}_3^2) \\ &+\Lambda\left[\tilde{\varkappa}_1^2\tilde{\varkappa}_2^2+\tilde{\varkappa}_1^2\tilde{\varkappa}_3^2+\tilde{\varkappa}_2^2\tilde{\varkappa}_3^2-\varkappa_1^2\varkappa_2^2-\varkappa_1^2\varkappa_3^2-\varkappa_2^2\varkappa_3^2\right] \\ &-\tilde{\varkappa}_1^2\left[\tilde{\varkappa}_2^2\tilde{\varkappa}_3^2-\varkappa_2^2\varkappa_3^2\right]+\varkappa_1^2\varkappa_2^2\tilde{\varkappa}_3^2+\varkappa_1^2\varkappa_3^2\tilde{\varkappa}_2^2-2\varkappa_1^2\varkappa_2^2\varkappa_3^2 = 0, \end{aligned} \tag{6.24}$$

where $\tilde{\varkappa}_i^2 = \varkappa_i^2+\alpha_i^2$.

Equation (6.24) can be presented as

$$\Lambda^3 - b\Lambda^2 + c\Lambda - d = 0, \tag{6.25}$$

where the coefficients b, c, and d are given by expressions (5.13)-(5.15).

Comparing polynomials (6.25) and (5.11), we note that the coefficients in front of the variables of the same powers are identical by the absolute value but alternate their signs. One can show, that in such a case the roots of the two polynomials are equal by the absolute value but have opposite signs. Hence, due to the definitions (5.23), we can readily

see that parameters λ_0^2, λ_1^2, and λ_2^2, given by equations (5.24)-(5.25), are also the three eigenvalues of the matrix $\mathbf{A}$.

As a result, the general solution for $E_1(z)$, for instance, is

$$E_1(z) = \tilde{c}_{10}e^{\lambda_0 z} + c_{10}e^{-\lambda_0 z} + \tilde{C}_1 e^{(\lambda+\mu i)z} + C_1 e^{(-\lambda+\mu i)z} + \tilde{C}_2 e^{(\lambda-\mu i)z} \tag{6.26}$$
$$+C_2 e^{(-\lambda-\mu i)z} = c_{10}e^{-\lambda_0 z} + C_1 e^{(-\lambda+\mu i)z} + C_2 e^{(-\lambda-\mu i)z},$$

where we leave only the terms with negative $\lambda_0 z$ and λz in the exponents due to the fact that λ_0 and λ are positive and the function $E(z)$ vanishes in the bulk.

For the field $E_1(z)$ to have a physical meaning, the coefficients C_1 and C_2 must be complex conjugate as well. From the system of equations (6.16) we can tell that the functions $E_2(z)$ and $E_3(z)$ are of a form similar to that of (6.26). We can therefore write the functions $E_i(z)$ as

$$E_1(z) = c_{10}e^{-\lambda_0 z} + (r_{11} + r_{12}i)\, e^{(-\lambda+\mu i)z} + (r_{11} - ri)\, e^{(-\lambda-\mu i)z} \tag{6.27}$$

$$E_2(z) = c_{20}e^{-\lambda_0 z} + (r_{21} + r_{22}i)\, e^{(-\lambda+\mu i)z} + (r_{21} - r_{22}i)\, e^{(-\lambda-\mu i)z} \tag{6.28}$$

$$E_3(z) = c_{30}e^{-\lambda_0 z} + (r_{31} + r_{32}i)\, e^{(-\lambda+\mu i)z} + (r_{31} - r_{32}i)\, e^{(-\lambda-\mu i)z} \tag{6.29}$$

Because the system (6.16) is homogeneous, we essentially have three unknown coefficients, for instance c_{10}, r_{11}, r_{12}, and we can use any pair of equations (6.16) to express the rest of the coefficients in terms of these unknowns. Using expressions (6.27) and equating the real and the imaginary parts of the coefficients in front of the same z-dependent functions on the LHS and RHS of equations (6.16), we obtain two system of equations - one for the coefficients in front of the functions $\exp[(-\lambda \pm \mu i)z]$ and one for the function $\exp[-\lambda_0 z]$. In the first case we have the following equations

$$\bar{\kappa}_1^2 r_{11} + 2\lambda\mu r_{12} - \varkappa_1^2 r_{21} - \varkappa_1^2 r_{31} = 0 \tag{6.30}$$
$$\bar{\kappa}_1^2 r_{12} - 2\lambda\mu r_{11} - \varkappa_1^2 r_{22} - \varkappa_1^2 r_{32} = 0 \tag{6.31}$$
$$\bar{\kappa}_2^2 r_{21} + 2\lambda\mu r_{22} - \varkappa_2^2 r_{11} - \varkappa_2^2 r_{31} = 0 \tag{6.32}$$
$$\bar{\kappa}_2^2 r_{22} - 2\lambda\mu r_{21} - \varkappa_2^2 r_{12} - \varkappa_2^2 r_{32} = 0 \tag{6.33}$$
$$\bar{\kappa}_3^2 r_{31} + 2\lambda\mu r_{32} - \varkappa_3^2 r_{11} - \varkappa_3^2 r_{21} = 0 \tag{6.34}$$
$$\bar{\kappa}_3^2 r_{32} - 2\lambda\mu r_{31} - \varkappa_3^2 r_{12} - \varkappa_3^2 r_{22} = 0, \tag{6.35}$$

where $\bar{\kappa}_j^2 = \lambda^2 - \mu^2 - \alpha_j^2 - \varkappa_j^2$.

We can pick any two pairs of these equations and the solution of this system will be the same. Choosing, for instance, the first two pairs, it is convenient to present coefficients r_{21}, r_{22}, r_{31}, r_{32} in terms of coefficients r_{11} and r_{12} as

$$r_{lm} = K_{lm}^{11} r_{11} + K_{lm}^{12} r_{12}, \tag{6.36}$$

where

$$K_{21}^{11} = \frac{\left(1 + \frac{\bar{\kappa}_1^2}{\varkappa_1^2} + \frac{(2\lambda\mu)^2}{\varkappa_1^2\left[\bar{\kappa}_2^2+\varkappa_2^2\right]}\right)}{\left(1 + \frac{\bar{\kappa}_2^2}{\varkappa_2^2} + \frac{(2\lambda\mu)^2}{\varkappa_2^2\left[\bar{\kappa}_2^2+\varkappa_2^2\right]}\right)} \tag{6.37}$$

$$K_{21}^{12} = \frac{\left(\frac{2\lambda\mu}{\varkappa_1^2} - \frac{2\lambda\mu\left(\bar{\kappa}_1^2+\varkappa_1^2\right)}{\left(\bar{\kappa}_2^2+\varkappa_2^2\right)\varkappa_1^2}\right)}{\left(1 + \frac{\bar{\kappa}_2^2}{\varkappa_2^2} + \frac{(2\lambda\mu)^2}{\varkappa_2^2\left[\bar{\kappa}_2^2+\varkappa_2^2\right]}\right)} \tag{6.38}$$

$$K_{22}^{11} = \frac{\varkappa_2^2}{\varkappa_2^2 + \bar{\kappa}_2^2}\left(-\frac{2\lambda\mu}{\varkappa_1^2} + \frac{2\lambda\mu}{\varkappa_2^2}K_{21}^{11}\right) \tag{6.39}$$

$$K_{22}^{12} = \frac{\varkappa_2^2}{\varkappa_2^2 + \bar{\kappa}_2^2}\left(\left[1 + \frac{\bar{\kappa}_1^2}{\varkappa_1^2}\right] + \frac{2\lambda\mu}{\varkappa_2^2}K_{21}^{12}\right) \tag{6.40}$$

$$K_{31}^{11} = \frac{1}{\varkappa_2^2}\left(-\varkappa_2^2 + \bar{\kappa}_2^2 K_{21}^{11} + 2\lambda\mu K_{22}^{11}\right) \tag{6.41}$$

$$K_{31}^{12} = \frac{1}{\varkappa_2^2}\left(\bar{\kappa}_2^2 K_{21}^{12} + 2\lambda\mu K_{22}^{12}\right) \tag{6.42}$$

$$K_{32}^{11} = \frac{1}{\varkappa_2^2}\left(\bar{\kappa}_2^2 K_{22}^{11} - 2\lambda\mu K_{21}^{11}\right) \tag{6.43}$$

$$K_{32}^{12} = \frac{1}{\varkappa_2^2}\left(-\varkappa_2^2 + \bar{\kappa}_2^2 K_{22}^{12} - 2\lambda\mu K_{21}^{12}\right) \tag{6.44}$$

$$\tag{6.45}$$

For the second system of equations we have three equations

$$\lambda_0^2 c_{10} = \left(\alpha_1^2 + \varkappa_1^2\right) c_{10} + \varkappa_1^2 \left(c_{20} + c_{30}\right) \tag{6.46}$$
$$\lambda_0^2 c_{20} = \left(\alpha_2^2 + \varkappa_2^2\right) c_{20} + \varkappa_2^2 \left(c_{10} + c_{30}\right) \tag{6.47}$$
$$\lambda_0^2 c_{30} = \left(\alpha_3^2 + \varkappa_3^2\right) c_{30} + \varkappa_3^2 \left(c_{20} + c_{10}\right). \tag{6.48}$$

Choosing any two of these equations, and due to the fact the determinant of the homogeneous system is zero, we can express the coefficients c_{20}

and c_{30} in terms of c_{10} as

$$c_{20} = K_{20}c_{10}, \qquad c_{30} = K_{30}c_{10.}, \tag{6.49}$$

$$K_{20} = \frac{(\lambda_0^2 - \alpha_1^2)\varkappa_2^2}{(\lambda_0^2 - \alpha_2^2)\varkappa_1^2} \tag{6.50}$$

$$K_{30} = \frac{(\lambda_0^2 - \alpha_1^2)}{\varkappa_1^2(\lambda_0^2 - \alpha_2^2)}\left(\lambda_0^2 - \alpha_2^2 - \varkappa_2^2\right) - 1. \tag{6.51}$$

The potentials $V_i(z)$ then have the form

$$V_i(z) = V_{ib} + \bar{r}_{i0}e^{-\lambda_0 z} + e^{-\lambda z}\left[(\lambda\bar{r}_{i1} - \mu\bar{r}_{i2})\cos\mu z - (\mu\bar{r}_{i1} + \lambda\bar{r}_{i2})\sin\mu z\right], \tag{6.52}$$

where $\bar{r}_{i0} = -c_{i0}/\lambda_0$, $\bar{r}_{ij} = 2r_{ij}/(\lambda^2 + \mu^2)$, $i = 1, 2, 3$, $j = 1, 2$.

In our earlier work [12] we showed that in the framework of the mean field approximation of the field theory formalism, for a multi-Yukawa fluid the so-called contact theorem [25, 26] holds true. According to this theorem, the density of the fluid at the wall is determined by the pressure of the fluid in the bulk, i.e.

$$\beta P = \rho(0_+), \tag{6.53}$$

where P is the pressure within the mean field approximation:

$$\beta P = \rho_b\left(1 + \frac{\varkappa_1^2}{2\alpha_1^2} + \frac{\varkappa_2^2}{2\alpha_2^2} + \frac{\varkappa_3^2}{2\alpha_3^2}\right). \tag{6.54}$$

The unknown coefficients $\bar{r}_{10}$, $\bar{r}_{11}$ and $\bar{r}_{12}$ can then be found from the boundary conditions given by the contact theorem (6.53). Setting $z = 0$ in Eq. (6.12), we obtain

$$V_{ib} - V_i(0) = \frac{\varkappa_i^2}{2\alpha_i^2}, \tag{6.55}$$

which results in a system of three equations

$$-\frac{\varkappa_1^2}{2\alpha_1^2} = \bar{r}_{10} + \lambda\bar{r}_{11} - \mu\bar{r}_{12}, \tag{6.56}$$

$$-\frac{\varkappa_2^2}{2\alpha_2^2} = \bar{r}_{20} + \lambda\bar{r}_{21} - \mu\bar{r}_{22}, \tag{6.57}$$

$$-\frac{\varkappa_3^2}{2\alpha_3^2} = \bar{r}_{30} + \lambda\bar{r}_{31} - \mu\bar{r}_{32}. \tag{6.58}$$

The solution of this system is

$$\bar{r}_{11} = \frac{-\frac{\varkappa_3^2}{2\alpha_3^2} + \frac{\varkappa_1^2}{2\alpha_1^2}K_{30} - A\left[\mu K_{30} + \lambda K_{31}^{12} - \mu K_{32}^{12}\right]}{-\lambda K_{30} + \lambda K_{31}^{11} - \mu K_{32}^{11} - B\left[\mu K_{30} + \lambda K_{31}^{12} - \mu K_{32}^{12}\right]} \tag{6.59}$$

$$\bar{r}_{12} = A - B\bar{r}_{11} \tag{6.60}$$

$$\bar{r}_{10} = -\frac{\varkappa_1^2}{2\alpha_1^2} - \lambda\bar{r}_{11} + \mu\bar{r}_{12} = -\frac{\varkappa_1^2}{2\alpha_1^2} + \mu A - \left[\lambda + \mu B\right]\bar{r}_{11}, \tag{6.61}$$

where

$$A = \frac{1}{\left[\mu K_{20} + \lambda K_{21}^{12} - \mu K_{22}^{12}\right]}\left[-\frac{\varkappa_2^2}{2\alpha_2^2} + \frac{\varkappa_1^2}{2\alpha_1^2}K_{20}\right], \tag{6.62}$$

$$B = \frac{1}{\left[\mu K_{20} + \lambda K_{21}^{12} - \mu K_{22}^{12}\right]}\left[-\lambda K_{20} + \lambda K_{21}^{11} - \mu K_{22}^{11}\right]. \tag{6.63}$$

Due to Eq. (6.12), the final expression for the linearized density profile is

$$\begin{aligned}\frac{\rho(z)}{\rho_b} &= 1 - \left[\bar{r}_{10} + \bar{r}_{20} + \bar{r}_{30}\right]e^{-\lambda_0 z} \\ &\quad - e^{-\lambda z}\Big[\left\{\lambda\left(\bar{r}_{11} + \bar{r}_{21} + \bar{r}_{31}\right) - \mu\left(\bar{r}_{12} + \bar{r}_{22} + \bar{r}_{32}\right)\right\}\cos\mu z \\ &\quad - \left\{\mu\left(\bar{r}_{11} + \bar{r}_{21} + \bar{r}_{31}\right) + \lambda\left(\bar{r}_{12} + \bar{r}_{22} + \bar{r}_{32}\right)\right\}\sin\mu z\Big].\end{aligned} \tag{6.64}$$

As was the case with the pair correlation function (5.35), the function on the RHS of Eq. (6.64) is defined by parameters λ_0, λ, and μ that shape the exponentially damped oscillatory behavior of the profile.

In Figures 16-23 we display density profile curves provided by the numerical solution of the mean field equation (6.12) (MF), the analytical expression (6.64) corresponding to the linearized mean field approximation (LMF), and test these results against Monte Carlo simulations data (MC). Due to the fact that the numerical solution requires the use of a cutoff radius, for comparison purposes we also present two estimations for the linearized profile with and without the respective value of that cutoff.

The results prove that theoretical predictions for the profile agree with the simulations very well. Moreover, the explicit analytical estimate (6.64) reproduces MC data better than the mean field solution. At high densities the agreement is the best for the first peak and deteriorates at distances farther away from the wall. In all the cases, as the temperature

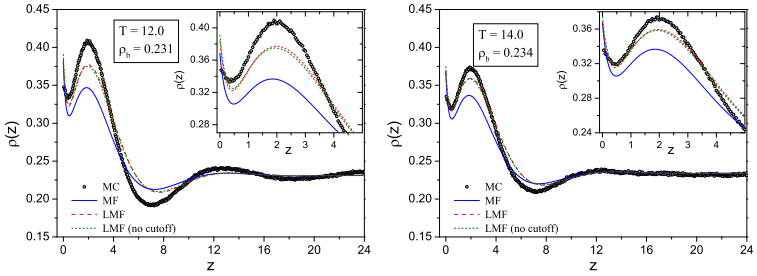

Figure 16. Density profiles for the Model M1. The dotted lines correspond to MC simulations; the blue solid lines come from the mean field solution (6.12); the dashed red and green lines correspond to analytical expression (6.64) with and without the cutoff radius, respectively.

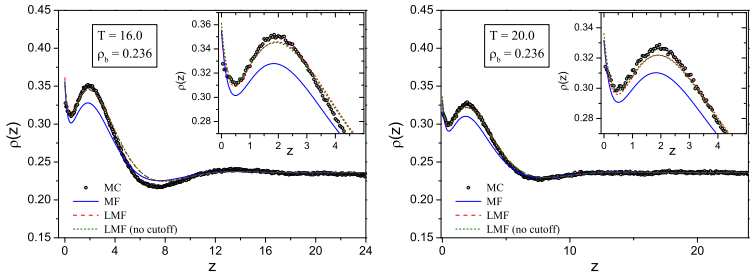

Figure 17. Same as in Figure (16) at higher temperatures.

rises the agreement between the theory and the simulations improves. Also, one can note that for all the densities and temperatures considered the theory reproduces very well the locations of the respective minima and maxima of the profile. For the Model M2 we observe significant discrepancy between the contact values of the density. This mismatch can likely be corrected by going beyond the mean field approximation and taking into account fluctuation effects as was done in our earlier study on a two-Yukawa fluid [10].

The behavior of the density profile is characterized by the split of the first maximum which leads to the formation of a distinct bi-layer close to the wall. We took note of this effect earlier in the Computer Simulations section as it was present also in the mesostructured systems we considered. The formation of the double peak can be explained by the

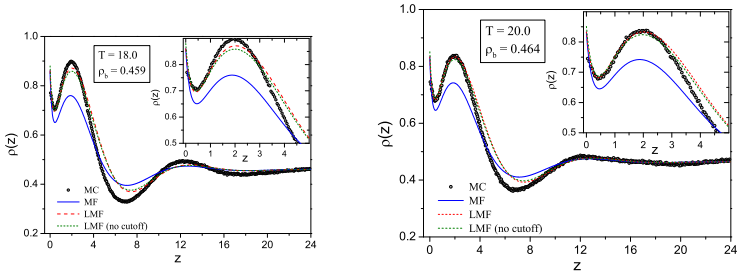

Figure 18. Same as in Figure (16) for higher densities and temperatures.

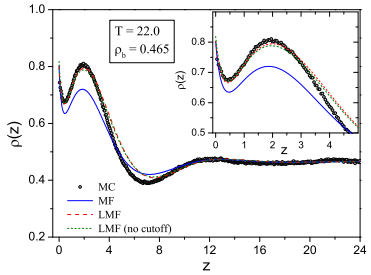

Figure 19. Same as in Figure (18).

attractive part of the SALR interaction potential as no similar behavior had been observed in the case of a 2Y fluid at a hard wall [10].

7. Conclusions

A fluid interacting with a three-Yukawa (3Y) potential was studied in the bulk and in the vicinity of a hard wall. The amplitudes and the ranges of the respective Yukawa terms were chosen so as to reproduce the short-range attraction and long-range repulsion (SALR) between particles, thus offering a different model of a system with competing interactions. A notable feature of this potential is the softness of the core, which describes the possibility of partial overlap between particles.

Two sets of parameter values for the three-Yukawa potential were considered to construct a SALR potential. A series of Monte-Carlo (MC) and Molecular Dynamics (MD) computer simulations across a wide range of

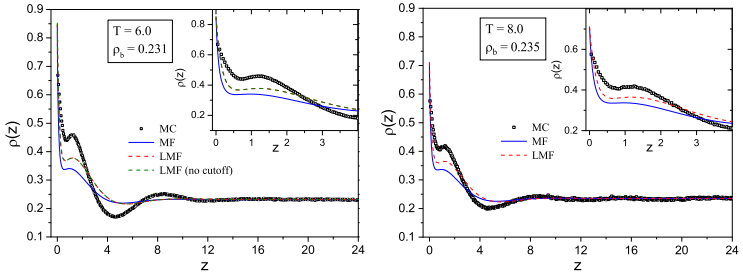

Figure 20. Same as in Figure (16) but for model M2.

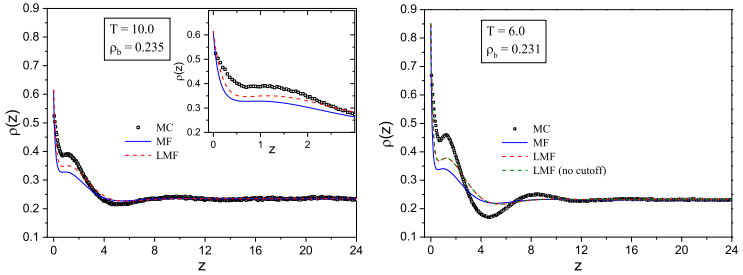

Figure 21. Same as in Figure (20).

temperatures and densities were performed. The results show that the model proposed can describe spontaneous appearance in the system of various mesostructures including lamellar and gyroidal phases, hexagonally packed cylindrical phases, cubically ordered and disordered clusters formed by particles or voids. Furthermore, we observed that these self-assembly effects become more pronounced when the fluid is confined between two inert walls, i.e. close to the walls cluster formation can occur at temperatures higher than those required for micro-segregation in the bulk. As the temperature increases, the clusters vanish, though distinct inhomogeneuity near the interface still persists.

A classical field theory was subsequently applied to describe the micro-structure and thermodynamics of a 3Y fluid at high temperatures and reproduce the density profiles obtained from our simulations. As a first step, we investigated the mesoscopically homogeneous phase in the bulk and close to a hard wall.

For the bulk region, a bicubic equation for generalized screening pa-

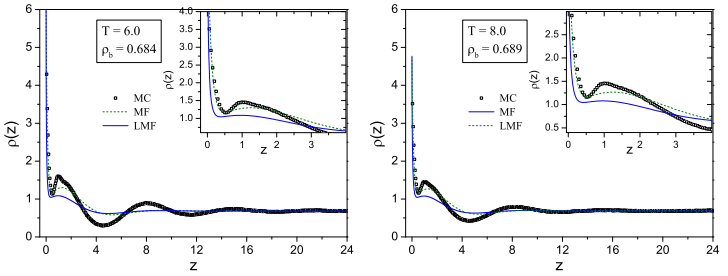

Figure 22. Same as in Figure (20) at higher densities.

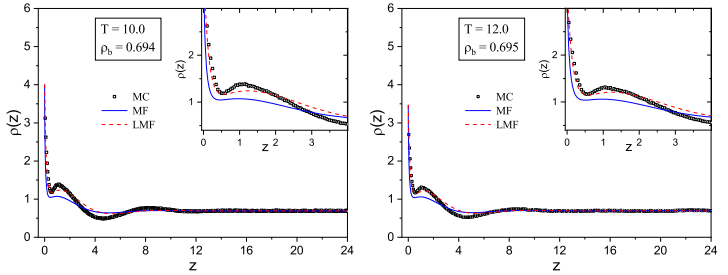

Figure 23. Same as in Figure (22).

rameters was derived and solved analytically. Based on these results, explicit analytical expressions for the radial distribution function were derived and compared to the MC data. Attempts to construct the respective phase diagram revealed that description of mesoscopic phases requires one to take into account excluded volume effects while a purely soft model in the random phase approximation leads to non-physical results. The structure factor was then calculated by introducing an effective hard core radius characteristic of the system. The λ-lines were subsequently constructed and phase behavior discussed. The results indicate that the model does indeed describe the possibility of spontaneous emergence of mesostructured phases in the system. Having the knowledge of the phase regions where the fluid is homogeneous, we therefore determined the conditions of applicability of the expressions for the structural properties derived from the field-theoretical approach. To this end, one should substitute the values of the density and the temperature above the λ-lines found. The location of these applicability regions is also sup-

ported by computer simulations data.

The microstructure of a 3Y-fluid in the vicinity of a hard wall was further investigated. In the framework of the mean field approximation an integral equation of the Euler-Lagrange type was obtained for the density profile. Linearization of this equation led to a system of second-order differential equations which were solved using the contact theorem as a boundary condition. The solution of these equations led to explicit analytical expressions for the density profile, which proved to be in very good agreement with the simulations data. Close to the wall we observed a characteristic split of the first maximum of the density profile. We relate the presence of this bilayer to the competing nature of the pair potential between particles, because this specific behavior had not been observed earlier in a simple attractive two-Yukawa fluid. The agreement between theoretical predictions for the profile and the MD simulations data improves with increasing temperature.

8. Acknowledgment

This work was supported by the National Research Foundation of Ukraine (Grant agreement No. 50/02.2020). The computer simulations have been performed on the computing cluster of the Institute for Condensed Matter Physics of NAS of Ukraine (Lviv, Ukraine).

References

1. J.-L. Bretonnet. AIMS Mater. Sci, 6(4), 509-548 (2019).
2. A. Ciach, Soft Matter, 14, 5497 (2019).
3. R. Roth, Mol. Phys. 109, 2897 (2011).
4. E.-Y. Kim, S.-C. Kim, and S.-H. Suh. Phys. Rev. E 85, 051203 (2012).
5. M. Litniewski and A. Ciach, J. Chem. Phys. 150, 234702 (2019).
6. A.J. Archer, N.B. Wilding, Phys. Rev., E76, 031501 (2007).
7. A.J. Archer, C. Ionescu, D. Pini, L. Reatto, J. Phys.: Condens. Matter, 20, 415106 (2008).
8. Y. Zhuang, K. Zhang, P. Charbonneau, Phys. Rev. Lett., 116, 098301. (2016).
9. D. Pini, A. Parola, Soft Matter, 13, 9259 (2017).
10. I. Kravtsiv, T. Patsahan, M. Holovko and D. Di Caprio. J. Chem. Phys. 142, 194708 (2015).
11. D. di Caprio, I. Kravtsiv, T. Patsahan, M. Holovko, Mol. Phys., 114, 2500 (2016).

12. D. Di Caprio, J. Stafiej, M. Holovko, I. Kravtsiv, Mol. Phys., 109, 695 (2011).
13. M. Holovko, D. Di Caprio, I. Kravtsiv, Condens. Matter Phys., 14, 33605 (2011).
14. M. Holovko, I. Kravtsiv and D. Di Caprio, Condens. Matter Phys. 16, 14002 (2013).
15. M. Holovko, T. Patsahan, I. Kravtsiv and D. Di Caprio, Condens. Matter Phys., 19, 13608 (2016).
16. D. Di Caprio, J. Stafiej and J.P. Badiali, Mol. Phys. 101, 2545 (2003).
17. D. Di Caprio, J. Stafiej and J.P. Badiali, J. Chem. Phys. 108, 8572 (1998).
18. D. Di Caprio, J. Stafiej and Z. Borkowska, J. Electroanal. Chem. 41, 582 (2005).
19. J.P. Hansen, I.R. McDonald, Theory of SimpleLiquids (Academic Press, Oxford, 2004).
20. Royall, C. P., Poon, W. C. K., Weeks, E. R. (2013). Soft Matter, 9(1), 17–27. doi:10.1039/c2sm26245b
21. Heyes, D. M., Okumura, H. (2006). Molecular Simulation, 32(1), 45–50. doi:10.1080/08927020500529442
22. S. Torquato. Random Heterogeneous Materials: Microstructure and Macroscopic Properties. Springer-Verlag (2002)
23. J.A. Barker and D. Henderson. Rev. Mod. Phys., 48, 587 (1976).
24. Y. Liu, W.-R. Chen, and S.-H. Chen, J. Chem. Phys. 122, 044507 (2005).
25. D. Henderson, L. Blum and J.L. Lebowitz, J. Electroanal. Chem. 102, 315 (1979).
26. M. Holovko, J.P. Badiali, D. di Caprio, J. Chem. Phys. 123, 234705 (2005).

CONDENSED MATTER PHYSICS

The journal **Condensed Matter Physics** is founded in 1993 and published by Institute for Condensed Matter Physics of the National Academy of Sciences of Ukraine.

AIMS AND SCOPE: The journal **Condensed Matter Physics** contains research and review articles in the field of statistical mechanics and condensed matter theory. The main attention is paid to physics of solid, liquid and amorphous systems, phase equilibria and phase transitions, thermal, structural, electric, magnetic and optical properties of condensed matter. Condensed Matter Physics is published quarterly.

ABSTRACTED/INDEXED IN: Chemical Abstract Service, Current Contents/Physical, Chemical&Earth Sciences; ISI Science Citation Index-Expanded, ISI Alerting Services; INSPEC; "Referatyvnyj Zhurnal"; "Dzherelo".

CONTACT INFORMATION:
Institute for Condensed Matter Physics
of the National Academy of Sciences of Ukraine
1 Svientsitskii Str., 79011 Lviv, Ukraine
Tel: +38(032)2761978; Fax: +38(032)2761158
E-mail: cmp@icmp.lviv.ua http://www.icmp.lviv.ua